Tension-free Dirac strings and steered magnetic charges in 3D artificial spin ice

Sabri Koraltan (sabri.koraltan@univie.ac.at)
University of Vienna https://orcid.org/0000-0002-1027-2232

Florian Slanovc
University of Vienna

Florian Bruckner
University of Vienna

Cristiano Nisoli
Los Alamos National Laboratory https://orcid.org/0000-0003-0053-1023

Andrii Chumak
University of Vienna https://orcid.org/0000-0001-5515-0848

Oleksandr Dobrovolskiy
University of Vienna https://orcid.org/0000-0002-7895-8265

Claas Abert
University of Vienna https://orcid.org/0000-0002-4999-0311

Dieter Suess
University of Vienna

Article

Keywords: condensed matter physics, photonics, biomedicine, spintronics, 3D magnetic networks

Posted Date: April 22nd, 2021

DOI: https://doi.org/10.21203/rs.3.rs-266861/v1

Version of Record: A version of this preprint was published at npj Computational Materials on August 5th, 2021. See the published version at https://doi.org/10.1038/s41524-021-00593-7.

Tension-free Dirac strings and steered magnetic charges in 3D artificial spin ice

Sabri Koraltan,[1,*] Florian Slanovc,[1] Florian Bruckner,[1] Cristiano Nisoli,[2]
Andrii V. Chumak,[3] Oleksandr V. Dobrovolskiy,[3] Claas Abert,[1,4] and Dieter Suess[1,4]

[1]*Physics of Functional Materials, Faculty of Physics, University of Vienna, Waehringer Strasse 17, 1090 Vienna, Austria*
[2]*Theoretical Division, Los Alamos National Laboratory, Los Alamos, NM, 87545, USA*
[3]*Nanomagnetics and Magnonics, Faculty of Physics, University of Vienna, Boltzmanngasse 5, 1090 Vienna, Austria*
[4]*University of Vienna Research Platform MMM Mathematics-Magnetism-Materials, University of Vienna, Austria*

(Dated: February 22, 2021)

3D nano-architectures present a new paradigm in modern condensed matter physics with numerous applications in photonics, biomedicine, and spintronics. They are promising for the realisation of 3D magnetic nanonetworks for ultra-fast and low-energy data storage. Frustration in these systems can lead to magnetic charges or magnetic monopoles, which can function as mobile, binary information carriers. However, Dirac strings in 2D artificial spin ices bind magnetic charges, while 3D dipolar counterparts require cryogenic temperatures for their stability. Here, we present a micromagnetic study of a highly-frustrated 3D artificial spin ice harboring tension-free Dirac strings with unbound magnetic charges at room temperature. We use micromagnetic simulations to demonstrate that the mobility threshold for magnetic charges is by 2 eV lower than their unbinding energy. By applying global magnetic fields, we steer magnetic charges in a given direction omitting unintended switchings. The introduced system paves a way towards 3D magnetic networks for data transport and storage.

INTRODUCTION

Data storage and transport devices ranging from hard disk drives to flash memories, from CMOS to spintronic technologies are of crucial importance in today's technological world. Usually, these devices are based on 2D structures approaching their limitations every day. 3D structures started to emerge over the past years, leading to significant improvements in both reducing the dimensions and increasing their efficiency, e.g. flash memories [1, 2]. In these data storage devices, the third dimension is used by the simple stacking of the same 2D structures. Thus, the whole power of the additional third dimension is not utilised.

Over the past years, spin ices, a class of 3D materials, have been investigated in detail. Spin ices are frustrated systems where the magnetic moments are residing on the sites of a pyrochlore lattice, a lattice with corner sharing tetrahedra, and commonly referred to as dipolar spin ices (DSI) [3–9]. Its degenerate ground state obeys the *ice-rule*, where two magnetic moments point to the center of the tetrahedra and two away from it. Switching a magnetic moment breaks the ice rule and creates a pair of magnetic charge in the centers of the vertices [5, 6]. These magnetic charges, commonly referred to as *emergent magnetic monopoles*, can be separated with a finite energy cost, and propagated through the lattice. In a classical analogue to Dirac's theory of magnetic monopoles [10], monopole motion in spin ice leaves a trace called a Dirac String (DS), which is simply the chain of flipped magnetic moments connecting the two separated positive and negative magnetic poles. Theoretical and experimental studies have shown that the energetic ground state is degenerate, constrained by the ice rule and that the magnetic monopoles are connected via Dirac Strings at low temperatures [3–8, 11, 12].

In order to study the geometrical frustrations and the magnetic charges on more controllable platform, 2D artificial spin ices (2DASIs) have been designed and investigated in detail [13–18]. There, lithographically patterned nanomagnets are arranged on different lattices. The most common ASI lattices are the square [19–22] and Kagome ices [23–26].

In contrast to DSI, the reduced dimensionality and geometric frustration in square ice lifts the degeneracy of the ice rule [14–18, 27, 28], thus limiting monopole mobility. Various methods have been explored to regain spin ice degeneracy, including quasi three-dimensional lattices [14, 16, 29–34] and interaction modifiers [35]. After early designs [30] and realizations [36] had envisioned a 3D artificial spin ice, the first three dimensional frustrated nanowire-lattice [37] was manufactured by two-photon lithography [38], in which charge propagation was later demonstrated [39]. However, in this lattice, the degeneracy of the ground state is still lifted, as the 3D structure consists of an interconnected nanowire-lattice. Additionally, the magnetic charges are connected via DS's, which store energy due to the presence of domain-walls at the vertex centers.

In this work, we combine the advantages of both DSI and ASI and present a 3D artificial spin ice (3DASI lattice), where numerical investigations are performed. Our lattice is a 3D nano-magnetic network of vertices consisting of four disconnected 3D magnetic ellipsoids with perfect Ising behavior enabling tension-free DS's and unbound magnetic charges by recovering the lost degeneracy of the ice rule obeying states. In this new lattice, we conserve the full accessibility of 2DASI and investigate numerically the propagation of emergent magnetic monopoles. We demonstrate that the difference in energy, required to create magnetic charges and their transport, is around 2 eV, which enables the controlled propagation of unbound charges. Considering the emergent magnetic monopoles as binary, mobile information carriers, the presented lattice demonstrates the steered motion of charge carriers in a 3D magnetic nano-network at room temperatures. The controllability of these charges paves a way towards a 3D magnetic network for data transport and storage.

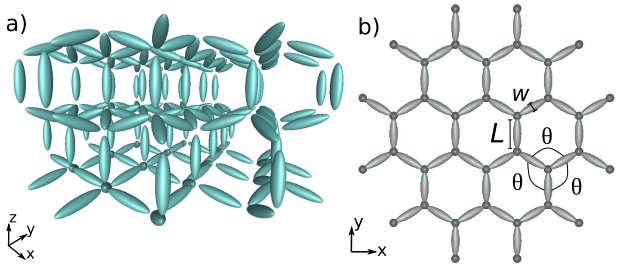

FIG. 1: **3DASI Lattice.**(a) 3D Illustration of the 3DASI lattice, and (b) the top view. The length of the ellipsoids L and maximal width W as well as the angle between the ellipsoids θ are depicted in (b).

Vertex type	$E_{dip}^{2D}(\mathrm{J_{NN}})$	$E_{dip}^{3D}(\mathrm{J_{NN}})$
Type I	$2(\sqrt{2}/3-2)$	$-5/(2\sqrt{3})$
Type II	$-2\sqrt{2}/3$	
Type III	0	0
Type IV	$2(\sqrt{2}/3+2)$	$15/(2\sqrt{3})$

TABLE I: Dipolar interaction energies in each vertex type in 2D and 3D ASI in units of J_{NN}, which is $J_{NN} \approx 1.72\,\mathrm{eV}$ for the chosen material and geometry parameters.

RESULTS

Modeling. In recent years, the direct-write technique of focused electron beam induced deposition (FEBID) has reached a high level of maturity for the 3D nanofabrication. Many complex-shaped nano-architectures have become available, providing access to experimental investigations of curvature-, geometry- and topology-induced effects in various disciplines, including magnetism, superconductivity, photonics and plasmonics [40–44].

Inspired by the recent developments in 3D optical lithography and focused particle 3D nano-printing by FEBID, we present a three dimensional ASI (3DASI) lattice, where magnetic rotational ellipsoids are arranged along the main axis of a tetrahedron, resulting in an angle $\theta = \arccos(-1/3) \approx 109.5^\circ$ between the elements, reproducing the Ice I_h crystal of the water ice [3, 5, 9]. Figure 1 illustrates the designed 3DASI lattice.

Note that in Fig. 1 we illustrate only the magnetic ellipsoids forming the lattice. In reality, the ellipsoids can be fabricated by direct-writing, i.e. FEBID, and interconnected with a magnetic insulator, e.g. platinum- [41] or niobium-based [45] compounds. We provide the illustration of a rather realistic fabrication model for one single vertex in the supplemental materials. With FEBID as a suitable nanofabrication technique of the 3DASI lattice, maximal width of the ellipsoids w can be reduced down to few tens of nanometers, while the length L can be chosen up to a few micrometers [40–43].

We choose rotational magnetic ellipsoids as ASI elements, because the self-demagnetizing field of the ellipsoids is homogeneous thus keeping the magnetic elements uniformly magnetized in the direction of the longer axis with no edge inhomogeneities [46–49]. Hence, our model shows nearly perfect Ising behavior and is suitable to separate and host magnetic charges. The maximal average deviation from a perfect uniformly magnetization for one ellipsoid in our model is found to be $\Delta\phi \approx 4\times10^{-4}\,\mathrm{deg}$, where the interactions with nearest and next-nearest neighbors were encountered.

In this work, we restrict our model to three layers to conduct numerical experiments in feasible times. However, we use the top and bottom layer rather as boundary conditions, while the region of interest is only the middle layer. In other words, we analyze the 3DASI lattice as a bulk system.

Dirac Strings and magnetic monopoles. Because of the symmetry of the tetrahedra, the degeneracy of the ice rule is not lifted in 3DASI. Consequently, the tension of the DS should vanish. To obtain an energy scale, we approximate the ellipsoids by magnetic dipoles with the dipole moment $\mu = M_s V$, where M_s is the saturation magnetization and V the volume of the nanostructure. In this formulation, the dipolar interaction energy for each pair of magnetic dipole moments $\mathbf{m}_i, \mathbf{m}_j$ at positions $\mathbf{r}_i, \mathbf{r}_j$ in the lattice is given by the dipolar interaction energy

$$E_{\mathrm{dip}} = \frac{\mu_0}{4\pi\left|\mathbf{r}_{ij}\right|^3}\left[\mathbf{m}_i\cdot\mathbf{m}_j - 3\frac{(\mathbf{m}_i\cdot\mathbf{r}_{ij})\,(\mathbf{m}_j\cdot\mathbf{r}_{ij})}{\left|\mathbf{r}_{ij}\right|^2}\right] \quad (1)$$

with $\mathbf{r}_{ij} := \mathbf{r}_j - \mathbf{r}_i$ and vacuum permeability μ_0. Then from Eq. (1) we obtain the energy scale

$$J_{NN} = \frac{3}{2\sqrt{2}}\frac{\mu_0}{\pi}\frac{\mu^2}{a^3} \quad (2)$$

as introduced in [49] , where a is the lattice constant.

From it we obtain the energy levels for the different vertex types, shown in Table I. Note the degeneracy in the ice rule obeying vertices.

Additionally, we perform calculations via micromagnetic simulations using `magnum.fe`[50] using material properties similar to the Cobalt-Iron(CoFe) alloys used in FEBID. Note that with this technique, the material parameters are already tunable [42, 51] for 2D structures, and advances are expected in the near future. We choose a saturation magnetization $M_s = 800\,\mathrm{kA/m}$ and exchange stiffness constant $A_{\mathrm{ex}} = 15.5\,\mathrm{pJ/m}$. The ellipsoids have the dimensions $L = 100\,\mathrm{nm}$, $w = 20\,\mathrm{nm}$ and a vertex-to-vertex distance of $a = 120\,\mathrm{nm}$. It is noteworthy that in our studies we especially focused on the 3D structures of sizes that have been demonstrated for platinum based nanofabrications. Magnetic CoFe/CoFeB structures are larger, but the down-scaling is expected within the next years.

Figure 2a) shows the calculated energies of all the possible vertices in 2DsASI and 3DASI. The latter show clearly the six-fold degeneracy of the ground state Type I/II. This degeneracy allows for magnetic charges to be separated, because a

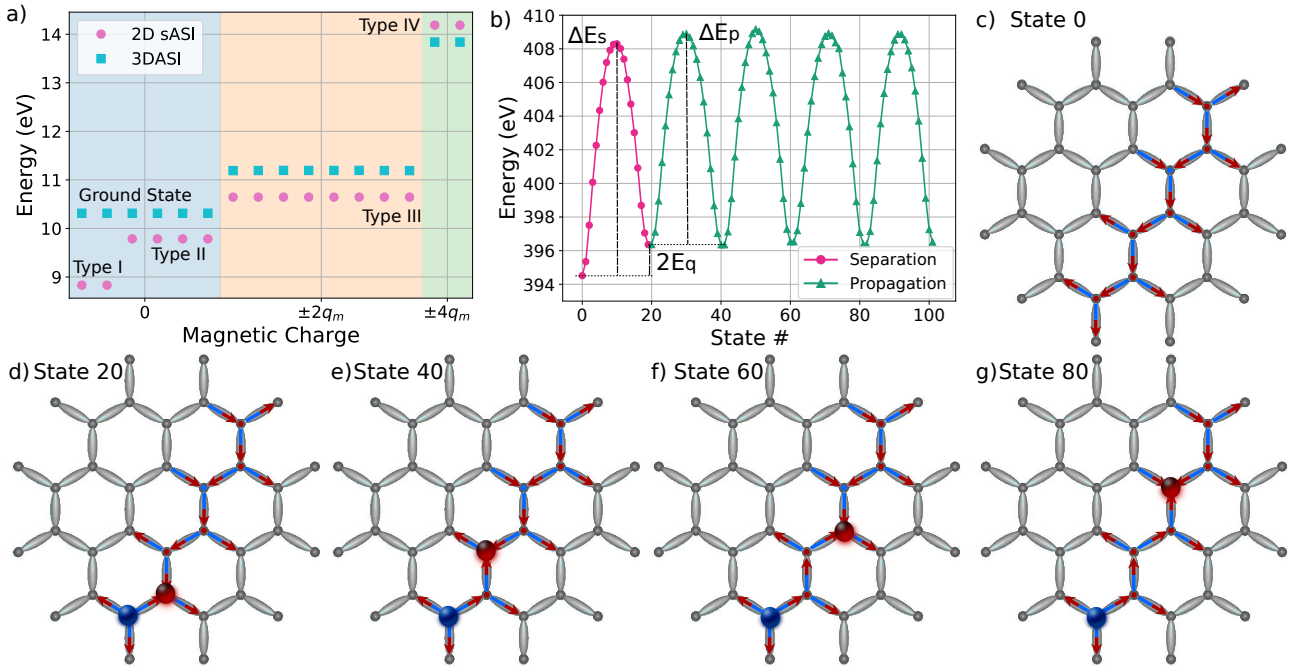

FIG. 2: **Magnetostatic energies and minimum energy paths for propagation and separation of charges.**(a) Total energies per vertex calculated with a micromagnetic treatment by taking into account energetic contributions of the exchange and demagnetization fields, where every possible magnetic configurations in a 2DsASI (circles) and in our 3DASI (squares) was considered. (b) Minimum energy paths to separate (magenta) the two magnetic charges by switching one ellipsoids magnetization in the ground state, and to propagate it further through the lattice in a constant direction (green). The difference of saddle points and the corresponding minima yields the separation barrier ΔE_s and propagation barrier ΔE_p, while energy of the lattice increases by $2E_q \approx 2\,\text{eV}$ due the two additional charge defects. (c) - (g) Schematic illustrations of the magnetization configurations for the ellipsoids in the Ds with the positive (dark red) and negative (dark blue) charged magnetic monopoles. Snapshots of magnetizations and animations available in the supplemental materials.

tension-free DS is created, making them *truly* unbound. In Fig. 2a), we chose to plot all $2^4 = 16$ possible configurations within a vertex. In reality, for vertices in the 3DASI lattice there exists only one unique ground state configuration, the ice-rule configuration, up to symmetry operations, i.e. rotations and mirroring, always obeying the *2in-2out* ice rule.

A more detailed description of the simulations, geometries and additional snapshots of magnetizations are given in the supplemental material.

According to the original definition of emergent magnetic monopoles, the energy required to create a monopole-antimonopole pair (charge separation), should be larger than the energy required to propagate it [6, 10, 16, 52–54]. We verify these properties by applying a full-micromagnetic model to calculate the energy barriers to separate and propagate the magnetic charges[48, 55, 56]. The detailed description of the full micromagnetic model and its application on 2DASIs is given in Ref. [48].

Figure 2b) illustrates the minimum energy paths (MEPs) for the switching processes within a DS. Starting from a lattice in the ground state, as illustrated in Fig. 2c), we separate two magnetic charges by switching the magnetization of one ellipsoid, and thus creating two Type III defects, which are depicted in Fig. 2d). The positive charge is then propagated to increase the length of the DS, shown in Figs. 2e)-g). It can be seen, that the separation MEP (magenta) yields an separation barrier ΔE_s approximately 2 eV higher than the propagation barriers ΔE_p (green MEPs), which are nearly constant. The reversal mechanisms are highly non-coherent and complex, being dictated by domain wall movements.

By separating the emergent monopoles, the energy of the system increases about $2E_q = 2\,\text{eV}$, which represents the energy increase due to Type III defects. Since we propagate only one charge, while the environment does not change, the energy of the system should stay constant during the propagation. However, we need to consider the possible Coulomb interactions between magnetic charges [5, 6]. In contrast to the classical DSI, this interaction can be neglected in comparison to the energy barriers in our 3DASI lattice [6].

Note that these results are obtained at $T = 0\,\text{K}$. In order to analyze the dependence of the stability and the propagation properties of a single monopole on both externally applied fields, and temperature, we use the arbitrary field finite temperature micromagnetic analysis (FTM) [57].

Arbitrary field finite temperature micromagnetic analysis. Starting from an initial magnetization state with one mag-

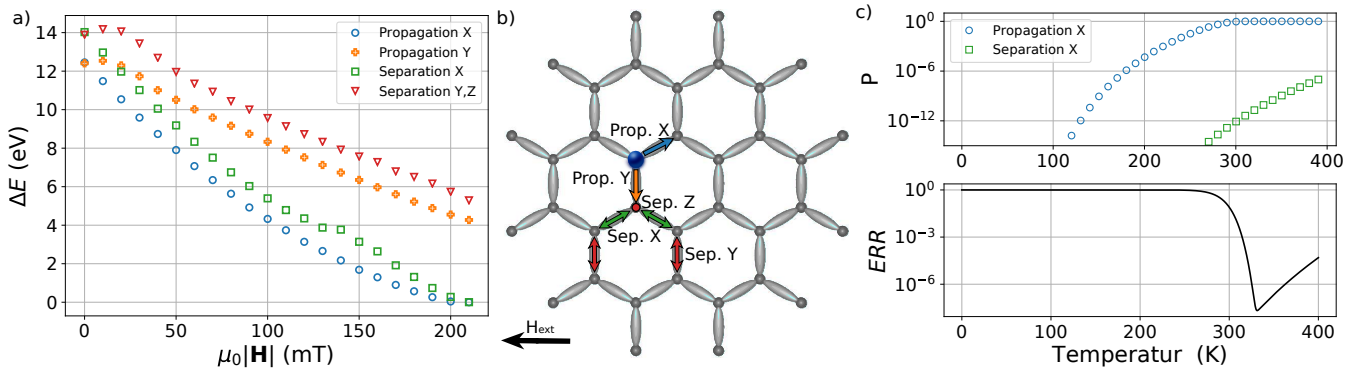

FIG. 3: **Arbitrary field finite temperature micromagnetic analysis.** a) Dependence of the energy barrier on the applied external fields at $T = 0\,\mathrm{K}$ to switch the magnetizations of different ellipsoids as depicted in (b). c) Upper panel: the switching probability P at different temperatures for the relevant transitions from (b) calculated with FTM-analysis, Eq. (3), where a Zeeman field with $\mu_0|\mathbf{H}| = 180\,\mathrm{mT}$, attempt frequency $f_0 = 50\,\mathrm{GHz}$ and pulse time $t_{\mathrm{final}} = 0.15\,\mathrm{ns}$ were chosen. Lower panel: mean error rate of successful propagation correlated with the unintended separation, as given by Eq. (4)

netic monopole of charge $Q = -2\,\mathrm{q_m}$, we calculate the energy barriers to switch the magnetization of different 3DASI elements under a uniform, external magnetic field with $\mu_0\mathbf{H} = -\mu_0|\mathbf{H}|\mathbf{e_x}$. Here, $\mu_0|\mathbf{H}|$ denotes the strength of the applied field, and $\mathbf{e_x}$ is the unit vector along x. $\mu_0|\mathbf{H}|$ is varied between $0 - 200\,\mathrm{mT}$.

The initial magnetization state is the same as in Fig. 4e). We consider different transitions, where the magnetic charge is propagated along x (blue arrow) and y (orange arrow), or additional charges are separated in a neighbored vertex, where the separation in three different directions is considered, x (green arrows), y and z (red), as illustrated in Fig. 3b). By doing so, we cover all possible transitions in our lattice, where the existing charges with $Q = -2\,\mathrm{q_m}$ are either propagated or new monopole-antimonopole pairs are separated at different locations.

Figure 3a) shows the calculated energy barriers as a function of the applied field strength for the transitions depicted in Fig. 3b). Our results indicate that the propagation barrier along X (blue, circles) is always lower than any other barrier. At vanishing fields, the barriers for propagation X and Y are equal, as demonstrated above. With the increasing field and approaching the coercive field, all barriers are lowering, ultimately, vanishing once the critical field is reached.

In the FTM analysis, described by Suess and co-workers in Ref. [57], a field-driven transition occurs with the switching probability

$$P = 1 - \exp\left(-f_0 t_{\mathrm{final}} e^{\left(\frac{-\Delta E(H)}{k_B T}\right)}\right), \qquad (3)$$

where f_0 denotes the attempt frequency, $\Delta E(H)$ the energy barrier at a given field magnitude, k_B the Boltzmann constant, t_{final} the time of applied field pulse and T is the temperature.

To analyze the stability of the propagation at room temperature, we consider $T = 300\,\mathrm{K}$ and calculate the associated probabilities where we choose $\mu_0|\mathbf{H}| = 180\,\mathrm{mT}$, $f_0 = 50\,\mathrm{GHz}$ and $t_{\mathrm{final}} = 0.15\,\mathrm{s}$. f_0 is chosen according to values considered in ASI literature [58], and t_{final} based on experimental expectations. Note that these two values appear only as a common factor in Eq. (3) and therefore other values for f_0 can always be compensated by an appropriate choice of t_{final}. The field strength $\mu_0|\mathbf{H}| = 180\,\mathrm{mT}$ is chosen such that the switching barrier of the propagation is below $300 k_B T$.

The upper panel of Fig. 3c) illustrates the relevant probabilities for the switching possibilities depicted in Fig. 3b). Our results indicate that only the element of interest will change its magnetization, as its switching probability increases with the temperature, where $P_{\mathrm{prop}}(300\,\mathrm{K}) > 0.9$. All the other probabilities are nearly zero at temperatures around $T = 300\,\mathrm{K}$. We chose to depict only the switching probabilities for the propagation and separation along x, as the other probabilities are lower than 1×10^{-15}.

However, we still need to define the mean switching error rate

$$\mathrm{ERR}(T) = 1 - P_{\mathrm{prop}}\left(1 - P_{\mathrm{sep}}(T)\right)^N, \qquad (4)$$

which describes the probability for an unsuccessful propagation, i.e. falsely switch of one element leading to a separation (or propagation failure due to insufficient thermal energy) in a lattice with N elements, where P_{prob} describes the propagation probabilities and P_{sep} the separation probabilities.

In the lower panel of Fig. 3 c) we see that the error rate significantly decreases after $T = 290\,\mathrm{K}$, as the X propagation probability increases to nearly 1. For $T > 330\,\mathrm{K}$ the propagation is guaranteed, however the separation probability increases leading to an increment in the mean error rate. This indicates that the monopoles can be propagated in a controlled manner, in the desired direction, and that they can be accessed at temperatures around room temperature, improving the scal-

ability and thermal stability of pyrochlore DSI.

Field-driven controlled monopole propagation. The controlled propagation can be achieved at any temperature, including $T = 0\,\mathrm{K}$, if one adjusts the strength, direction and duration of the globally applied magnetic fields. As illustrated in Fig. 3-a), the energy barrier vanishes for large enough fields. To investigate this in a rather direct manner, we conduct numerical experiments, where we continue with our micromagnetic treatment and investigate the propagation of monopoles by applying pulses of external magnetic fields at $T = 0\,\mathrm{K}$.

We start from an initial system where the middle layer is in the ground state. Reversing the magnetization in one boundary ellipsoid hosts exact one magnetic charge with $Q = -2q_m$, see Figs. 4c) and f). We continue by applying a magnetic field along $-x$ direction, as in the FTM analysis above. The field profile can be seen in Fig. 4a), where the magnitude of the applied field increases linearly over 4.8 ns from $160 - 208\,\mathrm{mT}$, and is then turned off abruptly after the propagation is successful. Note that we are confining the 3DASI lattice to avoid finite size effects, and analyze only the middle *bulk* layer.

Figure 4b) shows the temporal evolution of the averaged magnetization components within the middle layer. Our results indicate that the magnetic charge is propagated to the next vertex via domain wall movements as predicted by our string method calculations and FTM analysis. Magnetization snapshots at chosen times from Fig. 4h) shows that until the critical field is reached, small deviations from the ising state are observed for the ellipsoids in the ground state, explaining the slow decrease in the average $x-$component of the magnetization from Fig. 4b). Once the applied field is large enough, the propagation takes place keeping the other vertices in the ground state, avoiding additional charge separations. By turning off the external field, we relax all the ellipsoids back to their ising state and control the propagation by demand. One can see in Fig. 4b) that the average magnetization drops rather abruptly when the magnetic charge is propagated one vertex further with each step, demonstrating the free and controlled propagation of an unbound emergent charge in the presented lattice. In the supplemental materials we also demonstrate that the magnetic charge can be further propagated to the next x-row by applying the same protocol with a magnetic field along y.

DISCUSSION

We investigated micromagnetically a new 3DASI lattice, which combines the advantages of classical 2DASI and pyrochlore DSI lattices, recovering the lost frustration and degeneracy of the ground state of the 2DsASI by enabling tension-free Dirac Strings and thermally stable unbound magnetic monopoles. Due to large distances compared to the pyrochlore DSI, the Coulomb interactions between the charges are negligible. String method simulations and finite temperature micromagnetic analysis show that the lattice allows to create and propagate magnetic charges, which can exist freely or in pairs being connected via tension-free Dirac strings at arbitrary temperatures. We showed by numerical experiments, that a single unbound charge can be propagated through the lattice, without creating additional magnetic charges.

Low-energy and ultra-fast switching in the 3DASI lattice, as well as the stability of emergent magnetic monopoles at room temperature and above, paves a way towards functional 3D magnetic nano-networks for data transport and storage. The controlled propagation of the magnetic charges is of high interest regarding the idea of *magnetricity* [52, 59], which might lead to further new devices[18].

Even though we focused only on the center layer and therefore regarded our model as a bulk lattice, the limitations of the z layers, might show additional and equally interesting phenomena which will be investigated in detail in a further work. By *shaving off* at a given z dimension, the lattice would have magnetic vertices, containing only three ellipsoids, which would *always* host a magnetic charge. The top and bottom layers could act as charge plasma layers, which might *decharge* in the middle layer, creating a magnetic capacitor.

METHODS

String Method. For each switching process, we start from an initial state and a final state interconnected via 19-20 magnetization states, corresponding to a coherent rotation of the magnetization of the element of interest. In a second step, the total energy of each image is driven a small step towards its energetic minimum. The energy contributions are the demagnetization energy, the exchange energy and Zeeman energy (FTM analysis). The third step consists in cubic interpolation of the new path, such that the magnetization states are equidistant according to an appropriate energy norm [48, 50, 55]. The last two steps are repeated until convergence is reached.

Micromagnetic Simulations. By using the finite and boundary element method based simulation code `magnum.fe` [50], we solve the Landau-Lifshitz-Gilbert (LLG) equation [56]:

$$\frac{\partial \mathbf{m}}{\partial t} = -\frac{\gamma}{1+\alpha^2}\mathbf{m}\times\mathbf{H}^{\mathrm{eff}} - \frac{\alpha\gamma}{1+\alpha^2}\mathbf{m}\times\left(\mathbf{m}\times\mathbf{H}^{\mathrm{eff}}\right), \quad (5)$$

where α is the Gilbert damping constant, γ the reduced gyromagnetic ratio, $\mathbf{m}$ the magnetization unit vector, and $\mathbf{H}^{\mathrm{eff}}$ is the effective field term, which includes the considered energy contributions from demagnetizing, exchange, external and anisotropy fields (magnetic confinement). Vertex state energies are computed by calculating the demagnetizing and exchange energies from the relaxed structures (high damping $\alpha = 1$). For the field-driven dynamic simulations, we also include global external fields, and solve the LLG for a given time. Additionally, the magnetization components are averaged within the middle (bulk) layer for each time step, as depicted in Fig. 4b).

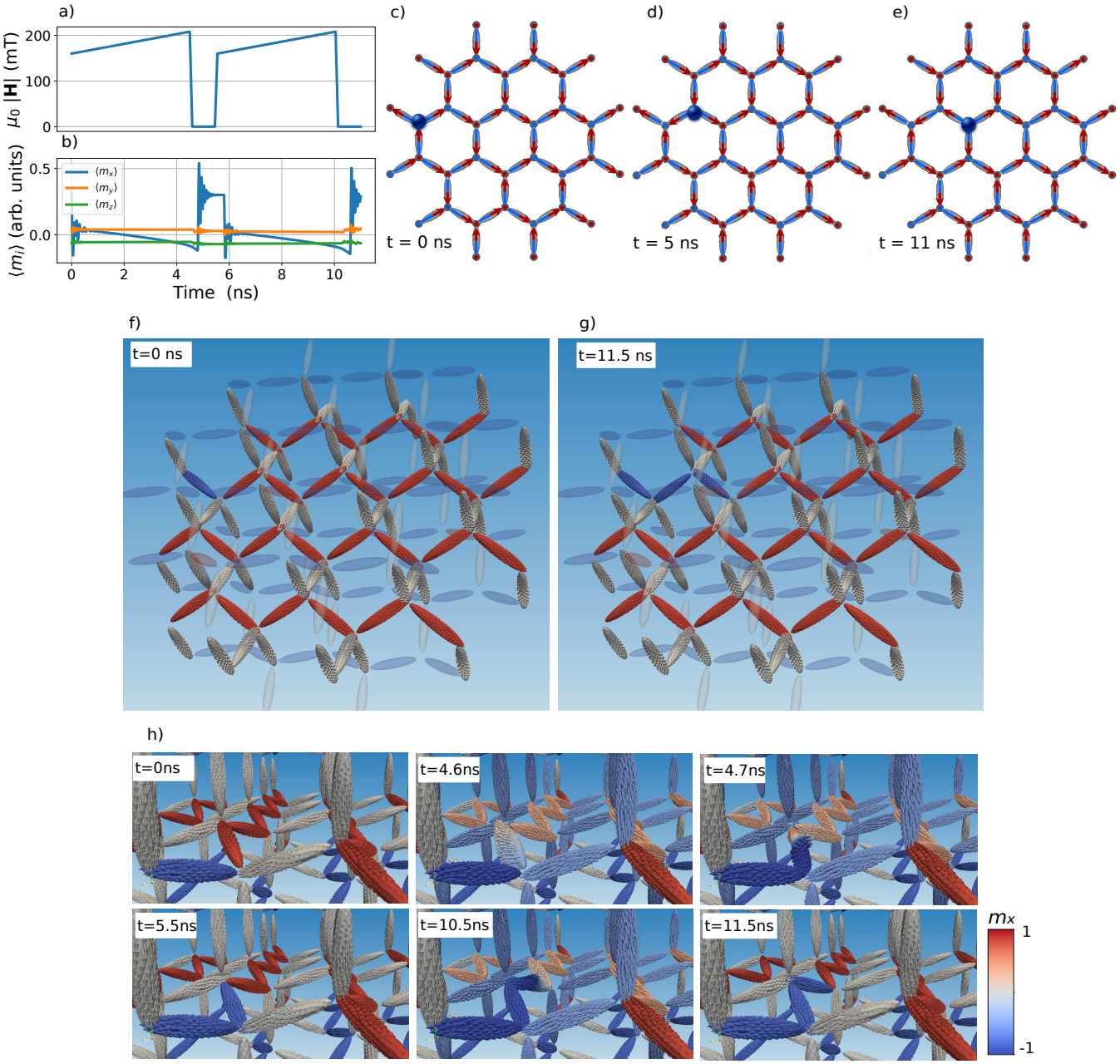

FIG. 4: **Field-driven monopole propagation.** Temporal evolution of the magnitude of the applied field (a) and of the averaged magnetization components (b) within the bulk layer during the x-propagation. The field is applied along $-x$ in order to maximize the Zeeman energy acting on the ellipsoid whose magnetization should be switched. The field is turned off after $t = 4.8$ ns in order to transfer the magnetic charge to the next vertex controlling the propagation. (c)-(e) Schematic illustration of the monopole (dark blue) propagation. (f)-(h) Snapshots of the magnetization states from the output of the conducted micromagnetic simulations, where f) illustrates the initial and g) the final magnetic configurations. The magnetization evolution during the simulations is depicted at different times (white boxes) in h). Color in f)-h) shows the x-component of the magnetization, as given by the colorbar.

ACKNOWLEDGEMENTS

We would like to thank Kevin Hofhuis and Johann Fischbacher for the fruitful discussions. The computational results presented have been achieved, in part, using the Vienna Scientific Cluster (VSC). S.K., C.A. A.V.C. and D.S. gratefully acknowledge the Austrian Science Fund (FWF) for support through Grant No. I 4917 (MagFunc). O.V.D. acknowledges the Austrian Science Fund (FWF) for support through

Grant No. I 4889 (CurviMag).

AUTHOR CONTRIBUTIONS

S.K. and F.S. conceived the concept. C.A. and F.B. wrote and improved the micromagnetic codes. S.K performed the micromagnetic simulations. S.K., F.S., F.B., C.N., A.V.C., O.V.D., C.A and D.S. further improved and developed the concept and discussed the results. All authors contributed to the manuscript.

COMPETING INTERESTS

The authors declare no competing interests.

ADDITIONAL INFORMATION

Supplementary information is available for this paper at .

Reprints and permission information is available at .

Correspondence and requests for materials should be addressed to S.K.

REFERENCES

* sabri.koraltan@univie.ac.at

[1] Min Zhu, Kun Ren, and Zhitang Song, "Ovonic threshold switching selectors for three-dimensional stackable phase-change memory," MRS Bulletin **44**, 715–720 (2019).

[2] B. Dieny, I. L. Prejbeanu, K. Garello, P. Gambardella, P. Freitas, R. Lehndorff, W. Raberg, U. Ebels, S. O. Demokritov, J. Akerman, A. Deac, P. Pirro, C. Adelmann, A. Anane, A. V. Chumak, A. Hirohata, S. Mangin, Sergio O. Valenzuela, M. Cengiz Onbaşlı, M. d'Aquino, G. Prenat, G. Finocchio, L. Lopez-Diaz, R. Chantrell, O. Chubykalo-Fesenko, and P. Bortolotti, "Opportunities and challenges for spintronics in the microelectronics industry," Nature Electronics **3**, 446–459 (2020).

[3] M J Harris, S T Bramwell, D F McMorrow, T Zeiske, and K W Godfrey, "Geometrical Frustration in the Ferromagnetic Pyrochlore Ho2Ti2O7," Phys. Rev. Lett. **79**, 4 (1997).

[4] S T Bramwell and M J Harris, "Frustration in Ising-type spin models on the pyrochlore lattice," J. Phys.: Condens. Matter **10**, L215–L220 (1998).

[5] I. A. Ryzhkin, "Magnetic relaxation in rare-earth oxide pyrochlores," J. Exp. Theor. Phys. **101**, 481–486 (2005).

[6] C. Castelnovo, R. Moessner, and S. L. Sondhi, "Magnetic monopoles in spin ice," Nature **451**, 42–45 (2008).

[7] D. J. P. Morris, D. A. Tennant, S. A. Grigera, B. Klemke, C. Castelnovo, R. Moessner, C. Czternasty, M. Meissner, K. C. Rule, J.-U. Hoffmann, K. Kiefer, S. Gerischer, D. Slobinsky, and R. S. Perry, "Dirac Strings and Magnetic Monopoles in the Spin Ice Dy2Ti2O7," Science **326**, 411–414 (2009).

[8] T. Fennell, P. P. Deen, A. R. Wildes, K. Schmalzl, D. Prabhakaran, A. T. Boothroyd, R. J. Aldus, D. F. McMorrow, and S. T. Bramwell, "Magnetic Coulomb Phase in the Spin Ice Ho2Ti2O7," Science **326**, 415–417 (2009).

[9] Steven T. Bramwell and Mark J. Harris, "The history of spin ice," J. Phys.: Condens. Matter **32**, 374010 (2020).

[10] Paul Adrien Maurice Dirac, "Quantised singularities in the electromagnetic field,," Proceedings of the Royal Society of London. Series A, Containing Papers of a Mathematical and Physical Character **133**, 60–72 (1931).

[11] K Matsuhira, Z Hiroi, T Tayama, S Takagi, and T Sakakibara, "A new macroscopically degenerate ground state in the spin ice compound Dy $_2$ Ti $_2$ O $_7$ under a magnetic field," J. Phys.: Condens. Matter **14**, L559–L565 (2002).

[12] M. I. Ryzhkin, I. A. Ryzhkin, and S. T. Bramwell, "Dynamic susceptibility and dynamic correlations in spin ice," EPL **104**, 37005 (2013).

[13] R. F. Wang, C. Nisoli, R. S. Freitas, J. Li, W. McConville, B. J. Cooley, M. S. Lund, N. Samarth, C. Leighton, V. H. Crespi, and P. Schiffer, "Artificial 'spin ice' in a geometrically frustrated lattice of nanoscale ferromagnetic islands," Nature **439**, 303–306 (2006).

[14] G. Möller and R. Moessner, "Artificial Square Ice and Related Dipolar Nanoarrays," Phys. Rev. Lett. **96**, 237202 (2006).

[15] L. A. Mól, R. L. Silva, R. C. Silva, A. R. Pereira, W. A. Moura-Melo, and B. V. Costa, "Magnetic monopole and string excitations in two-dimensional spin ice," Journal of Applied Physics **106**, 063913 (2009).

[16] L. A. S. Mól, W. A. Moura-Melo, and A. R. Pereira, "Conditions for free magnetic monopoles in nanoscale square arrays of dipolar spin ice," Phys. Rev. B **82**, 054434 (2010).

[17] Cristiano Nisoli, Roderich Moessner, and Peter Schiffer, "Colloquium: Artificial spin ice: Designing and imaging magnetic frustration," Rev. Mod. Phys. **85**, 1473–1490 (2013).

[18] Sandra H. Skjærvø, Christopher H. Marrows, Robert L. Stamps, and Laura J. Heyderman, "Advances in artificial spin ice," Nature Reviews Physics **2**, 13–28 (2020).

[19] Cristiano Nisoli, Ruifang Wang, Jie Li, William F. McConville, Paul E. Lammert, Peter Schiffer, and Vincent H. Crespi, "Ground State Lost but Degeneracy Found: The Effective Thermodynamics of Artificial Spin Ice," Phys. Rev. Lett. **98**, 217203 (2007).

[20] Vassilios Kapaklis, Unnar B Arnalds, Adam Harman-Clarke, Evangelos Th Papaioannou, Masoud Karimipour, Panagiotis Korelis, Andrea Taroni, Peter C W Holdsworth, Steven T Bramwell, and Björgvin Hjörvarsson, "Melting artificial spin ice," New J. Phys. **14**, 035009 (2012).

[21] Vassilios Kapaklis, Unnar B. Arnalds, Alan Farhan, Rajesh V. Chopdekar, Ana Balan, Andreas Scholl, Laura J. Heyderman, and Björgvin Hjörvarsson, "Thermal fluctuations in artificial spin ice," Nature Nanotechnology **9**, 514–519 (2014).

[22] A. Farhan, P. M. Derlet, A. Kleibert, A. Balan, R. V. Chopdekar, M. Wyss, J. Perron, A. Scholl, F. Nolting, and L. J. Heyderman, "Direct Observation of Thermal Relaxation in Artificial Spin Ice," Phys. Rev. Lett. **111**, 057204 (2013).

[23] A. Farhan, P. M. Derlet, L. Anghinolfi, A. Kleibert, and L. J. Heyderman, "Magnetic charge and moment dynamics in artificial kagome spin ice," Phys. Rev. B **96**, 064409 (2017).

[24] Yi Qi, T. Brintlinger, and John Cumings, "Direct observation of the ice rule in an artificial kagome spin ice," Phys. Rev. B **77**, 094418 (2008).

[25] Unnar B. Arnalds, Alan Farhan, Rajesh V. Chopdekar, Vassilios Kapaklis, Ana Balan, Evangelos Th. Papaioannou, Martina Ahlberg, Frithjof Nolting, Laura J. Heyderman, and Björgvin Hjörvarsson, "Thermalized ground state of artificial kagome spin ice building blocks," Appl. Phys. Lett. **101**, 112404 (2012).

[26] Kevin Hofhuis, Aleš Hrabec, Hanu Arava, Naëmi Leo, Yen-Lin Huang, Rajesh V. Chopdekar, Sergii Parchenko, Armin

Kleibert, Sabri Koraltan, Claas Abert, Christoph Vogler, Dieter Suess, Peter M. Derlet, and Laura J. Heyderman, "Thermally superactive artificial kagome spin ice structures obtained with the interfacial Dzyaloshinskii-Moriya interaction," Phys. Rev. B **102**, 180405 (2020).

[27] Gia-Wei Chern, Muir J. Morrison, and Cristiano Nisoli, "Degeneracy and Criticality from Emergent Frustration in Artificial Spin Ice," Phys. Rev. Lett. **111**, 177201 (2013).

[28] Cristiano Nisoli, "Equilibrium field theory of magnetic monopoles in degenerate square spin ice: Correlations, entropic interactions, and charge screening regimes," Phys. Rev. B **102**, 220401 (2020).

[29] Alan Farhan, Michael Saccone, Charlotte F. Petersen, Scott Dhuey, Rajesh V. Chopdekar, Yen-Lin Huang, Noah Kent, Zuhuang Chen, Mikko J. Alava, Thomas Lippert, Andreas Scholl, and Sebastiaan van Dijken, "Emergent magnetic monopole dynamics in macroscopically degenerate artificial spin ice," Science Advances **5**, eaav6380 (2019).

[30] Gia-Wei Chern, Charles Reichhardt, and Cristiano Nisoli, "Realizing three-dimensional artificial spin ice by stacking planar nano-arrays," Appl. Phys. Lett. **104**, 013101 (2014).

[31] D Thonig, S Reißaus, I Mertig, and J Henk, "Thermal string excitations in artificial spin-ice square dipolar arrays," J. Phys.: Condens. Matter **26**, 266006 (2014).

[32] Yann Perrin, Benjamin Canals, and Nicolas Rougemaille, "Extensive degeneracy, Coulomb phase and magnetic monopoles in artificial square ice," Nature **540**, 410–413 (2016).

[33] Alan Farhan, Michael Saccone, Charlotte F. Petersen, Scott Dhuey, Kevin Hofhuis, Rhodri Mansell, Rajesh V. Chopdekar, Andreas Scholl, Thomas Lippert, and Sebastiaan van Dijken, "Geometrical frustration and planar triangular antiferromagnetism in quasi-three-dimensional artificial spin architecture," Phys. Rev. Lett. **125**, 267203 (2020).

[34] A. A. Mistonov, I. S. Dubitskiy, I. S. Shishkin, N. A. Grigoryeva, A. Heinemann, N. A. Sapoletova, G. A. Valkovskiy, and S. V. Grigoriev, "Magnetic structure of the inverse opal-like structures: Small angle neutron diffraction and micromagnetic simulations," Journal of Magnetism and Magnetic Materials **477**, 99–108 (2019).

[35] Erik Östman, Henry Stopfel, Ioan-Augustin Chioar, Unnar B Arnalds, Aaron Stein, Vassilios Kapaklis, and Björgvin Hjörvarsson, "Interaction modifiers in artificial spin ices," Nature Physics **14**, 375–379 (2018).

[36] AA Mistonov, NA Grigoryeva, AV Chumakova, H Eckerlebe, NA Sapoletova, KS Napolskii, AA Eliseev, D Menzel, and SV Grigoriev, "Three-dimensional artificial spin ice in nanostructured co on an inverse opal-like lattice," Physical Review B **87**, 220408 (2013).

[37] Andrew May, Matthew Hunt, Arjen Van Den Berg, Alaa Hejazi, and Sam Ladak, "Realisation of a frustrated 3D magnetic nanowire lattice," Communications Physics **2**, 1–9 (2019).

[38] Gwilym Williams, Matthew Hunt, Benedikt Boehm, Andrew May, Michael Taverne, Daniel Ho, Sean Giblin, Dan Read, John Rarity, Rolf Allenspach, and Sam Ladak, "Two-photon lithography for 3D magnetic nanostructure fabrication," Nano Res. **11**, 845–854 (2018).

[39] Andrew May, Michael Saccone, Arjen van den Berg, Joseph Askey, Matthew Hunt, and Sam Ladak, "Magnetic charge propagation upon a 3d artificial spin-ice," arXiv:2007.07618.

[40] Amalio Fernández-Pacheco, Luka Skoric, José María De Teresa, Javier Pablo-Navarro, Michael Huth, and Oleksandr V. Dobrovolskiy, "Writing 3D Nanomagnets Using Focused Electron Beams," Materials **13**, 3774 (2020).

[41] Lukas Keller, Mohanad K. I. Al Mamoori, Jonathan Pieper, Christian Gspan, Irina Stockem, Christian Schröder, Sven Barth, Robert Winkler, Harald Plank, Merlin Pohlit, Jens Müller, and Michael Huth, "Direct-write of free-form building blocks for artificial magnetic 3D lattices," Scientific Reports **8**, 6160 (2018).

[42] Oleksandr V. Dobrovolskiy, Sergey A. Bunyaev, Nikolay R. Vovk, David Navas, Pawel Gruszecki, Maciej Krawczyk, Roland Sachser, Michael Huth, Andrii V. Chumak, Konstantin Y. Guslienko, and Gleb N. Kakazei, "Spin-wave spectroscopy of individual ferromagnetic nanodisks," Nanoscale **12**, 21207–21217 (2020).

[43] M. Huth, F. Porrati, and O. V. Dobrovolskiy, "Focused electron beam induced deposition meets materials science," Microelectronic Engineering **185-186**, 9–28 (2018).

[44] Amalio Fernández-Pacheco, Robert Streubel, Olivier Fruchart, Riccardo Hertel, Peter Fischer, and Russell P. Cowburn, "Three-dimensional nanomagnetism," Nature Communications **8**, 15756 (2017).

[45] Fabrizio Porrati, Sven Barth, Roland Sachser, Oleksandr V. Dobrovolskiy, Anja Seybert, Achilleas S. Frangakis, and Michael Huth, "Crystalline Niobium Carbide Superconducting Nanowires Prepared by Focused Ion Beam Direct Writing," ACS Nano **13**, 6287–6296 (2019).

[46] J. A. Osborn, "Demagnetizing Factors of the General Ellipsoid," Phys. Rev. **67**, 351–357 (1945).

[47] N Rougemaille, F Montaigne, B Canals, M Hehn, H Riahi, D Lacour, and J-C Toussaint, "Chiral nature of magnetic monopoles in artificial spin ice," New J. Phys. **15**, 035026 (2013).

[48] Sabri Koraltan, Matteo Pancaldi, Naëmi Leo, Claas Abert, Christoph Vogler, Kevin Hofhuis, Florian Slanovc, Florian Bruckner, Paul Heistracher, Matteo Menniti, Paolo Vavassori, and Dieter Suess, "Dependence of energy barrier reduction on collective excitations in square artificial spin ice: A comprehensive comparison of simulation techniques," Phys. Rev. B **102**, 064410 (2020).

[49] Naëmi Leo, Matteo Pancaldi, Sabri Koraltan, Pedro Villalba González, Claas Abert, Christoph Vogler, Florian Slanovc, Florian Bruckner, Paul Heistracher, Kevin Hofhuis, Matteo Menniti, Dieter Suess, and Paolo Vavassori, "Chiral switching and dynamic barrier reductions in artificial square ice," New J. Phys (2021).

[50] Claas Abert, Lukas Exl, Florian Bruckner, André Drews, and Dieter Suess, "magnum.fe: A micromagnetic finite-element simulation code based on FEniCS," Journal of Magnetism and Magnetic Materials **345**, 29–35 (2013).

[51] S. A. Bunyaev, B. Budinska, R. Sachser, Q. Wang, K. Levchenko, S. Knauer, A. V. Bondarenko, M. Urbanek, K. Y. Guslienko, A. V. Chumak, M. Huth, G. N. Kakazei, and O. V. Dobrovolskiy, "Engineered magnetization and exchange stiffness in direct-write co-fe nanoelements," arXiv:2012.01481.

[52] E. Y. Vedmedenko, "Dynamics of bound monopoles in artificial spin ice: How to store energy in dirac strings," Phys. Rev. Lett. **116**, 077202 (2016).

[53] L. D. C. Jaubert and P. C. W. Holdsworth, "Signature of magnetic monopole and Dirac string dynamics in spin ice," Nature Physics **5**, 258–261 (2009).

[54] L. D. C. Jaubert and P. C. W. Holdsworth, "Magnetic monopole dynamics in spin ice," J. Phys.: Condens. Matter **23**, 164222 (2011).

[55] Weinan E, Weiqing Ren, and Eric Vanden-Eijnden, "Simplified and improved string method for computing the minimum energy paths in barrier-crossing events," The Journal of Chemical Physics **126**, 164103 (2007).

[56] Claas Abert, "Micromagnetics and spintronics: models and numerical methods," Eur. Phys. J. B **92**, 120 (2019).

[57] D. Suess, L. Breth, J. Lee, M. Fuger, C. Vogler, F. Bruckner, B. Bergmair, T. Huber, J. Fidler, and T. Schrefl, "Calculation of coercivity of magnetic nanostructures at finite temperatures," Phys. Rev. B **84**, 224421 (2011).

[58] A. Farhan, P. M. Derlet, A. Kleibert, A. Balan, R. V. Chopdekar, M. Wyss, L. Anghinolfi, F. Nolting, and L. J. Heyderman, "Exploring hyper-cubic energy landscapes in thermally active finite artificial spin-ice systems," Nature Phys **9**, 375–382 (2013).

[59] H. Arava, E. Y. Vedmedenko, J. Cui, J. Vijayakumar, A. Kleibert, and L. J. Heyderman, "Control of emergent magnetic monopole currents in artificial spin ice," Phys. Rev. B **102**, 144413 (2020).

Figures

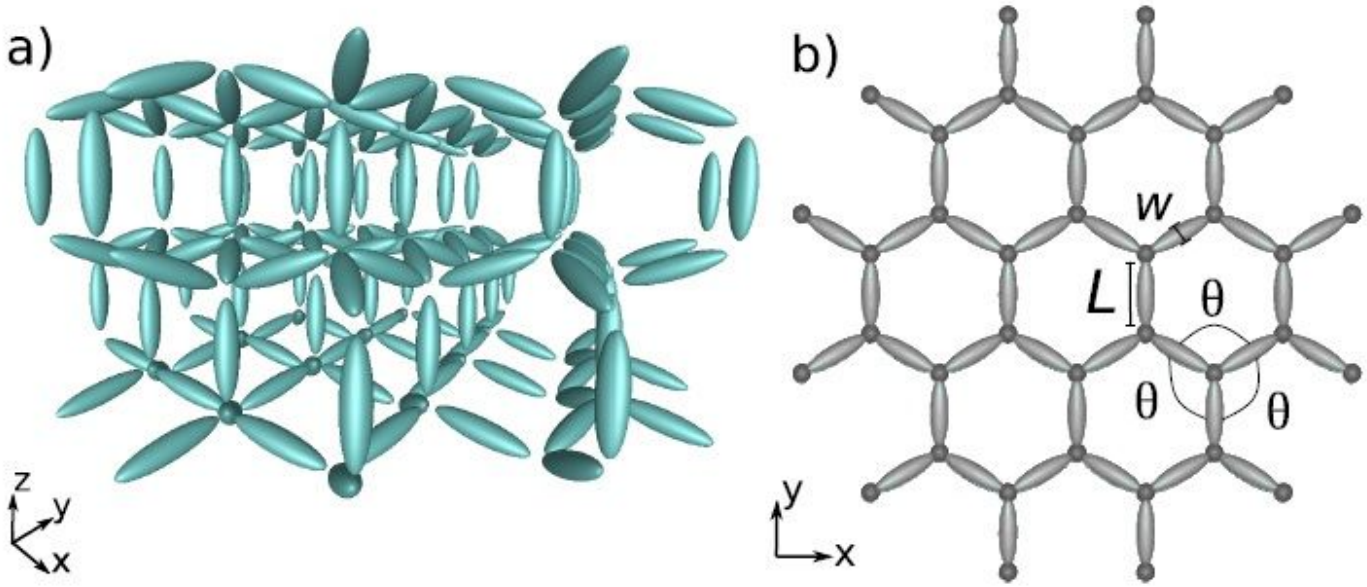

Figure 1

3DASI Lattice.(a) 3D Illustration of the 3DASI lattice, and (b) the top view. The length of the ellipsoids L and maximal widthW as well as the angle between the ellipsoids q are depicted in (b).

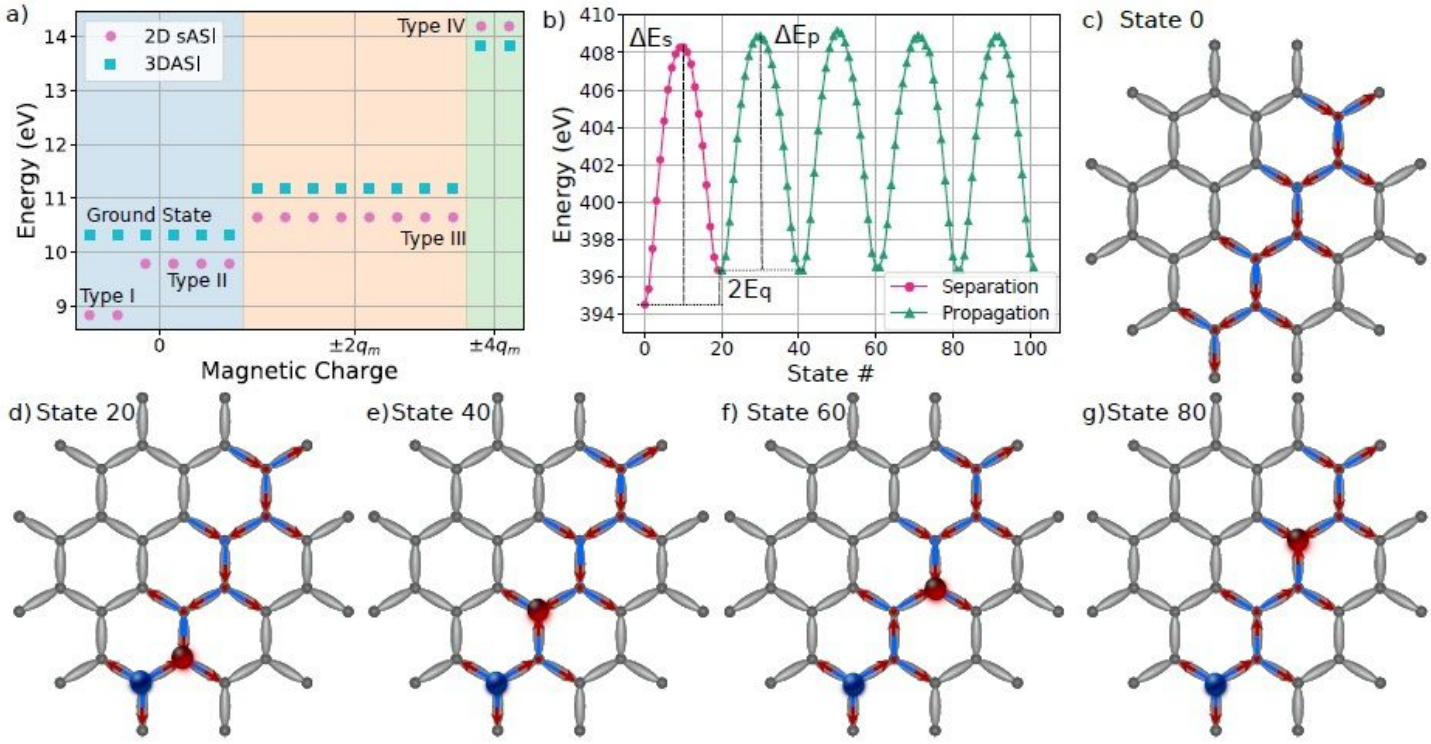

Figure 2

Magnetostatic energies and minimum energy paths for propagation and separation of charges.(a) Total energies per vertex calculated with a micromagnetic treatment by taking into account energetic contributions of the exchange and demagnetization fields, where every possible magnetic configurations in a 2DsASI (circles) and in our 3DASI (squares) was considered. (b) Minimum energy paths to separate (magenta) the two magnetic charges by switching one ellipsoids magnetization in the ground state, and to propagate it further through the lattice in a constant direction (green). The difference of saddle points and the corresponding minima yields the separation barrier DEs and propagation barrier DEp, while energy of the lattice increases by 2Eq ~2eV due the two additional charge defects. (c) - (g) Schematic illustrations of the magnetization configurations for the ellipsoids in the Ds with the positive (dark red) and negative (dark blue) charged magnetic monopoles. Snapshots of magnetizations and animations available in the supplemental materials.

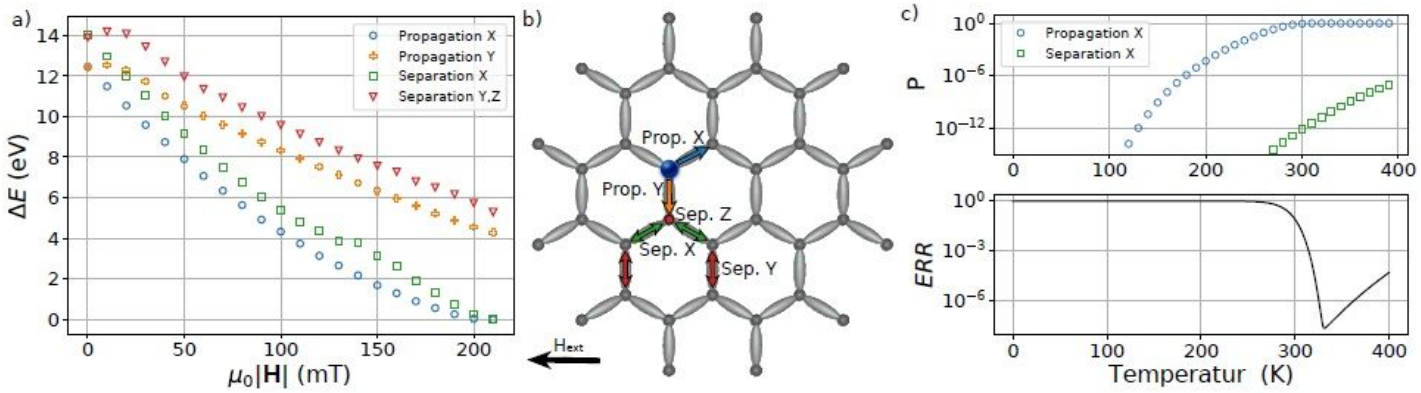

Figure 3

Arbitrary field finite temperature micromagnetic analysis. a) Dependence of the energy barrier on the applied external fields at T = 0K to switch the magnetizations of different ellipsoids as depicted in (b). c) Upper panel: the switching probability P at different temperatures for the relevant transitions from (b) calculated with FTM-analysis, Eq. (3), where a Zeeman field with m0jHj = 180mT, attempt frequency f0 = 50GHz and pulse time tfinal = 0:15ns were chosen. Lower panel: mean error rate of successful propagation correlated with the unintended separation, as given by Eq. (4)

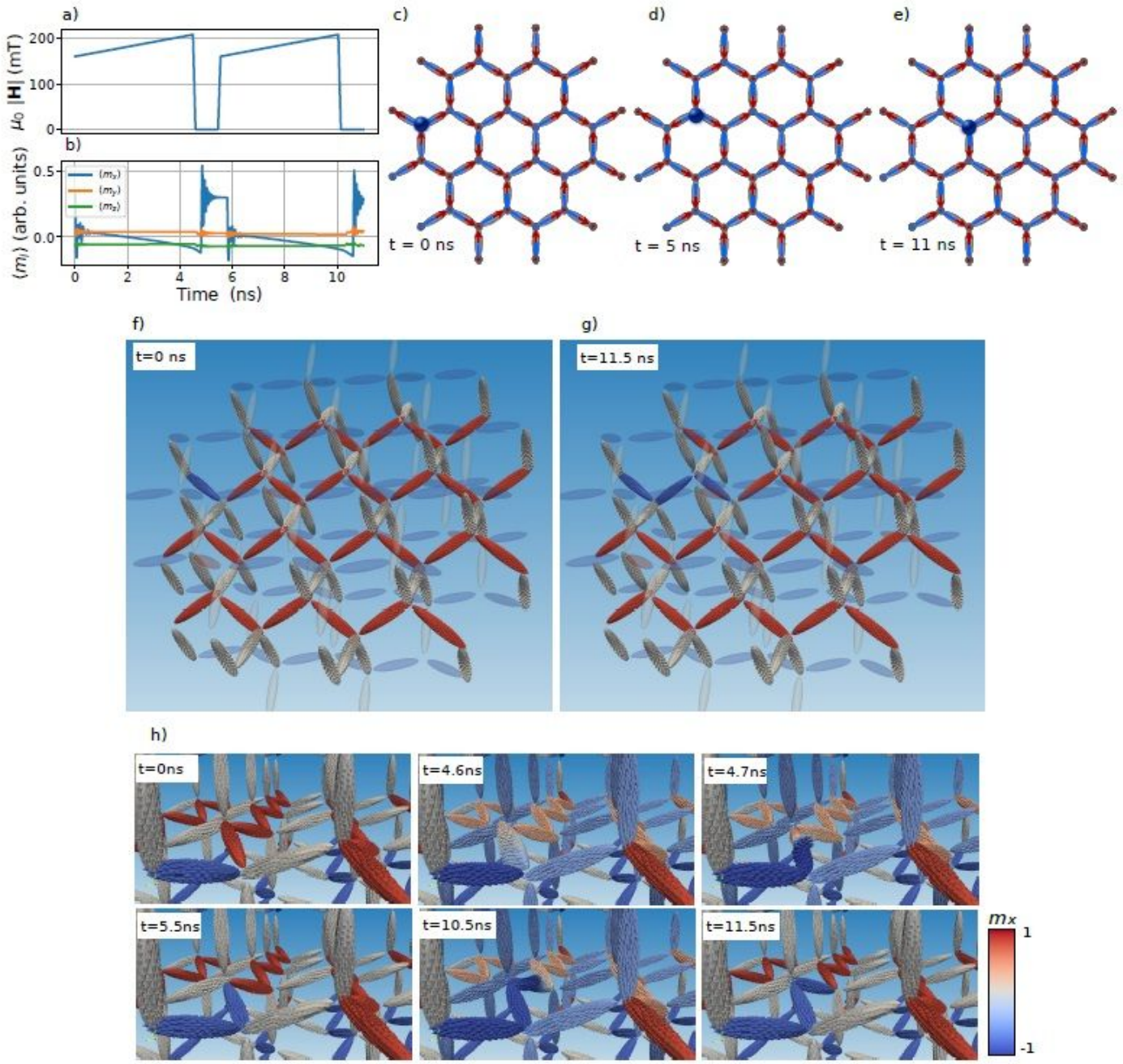

Figure 4

Field-driven monopole propagation. Temporal evolution of the magnitude of the applied field (a) and of the averaged magnetization components (b) within the bulk layer during the x-propagation. The field is applied along x in order to maximize the Zeeman energy acting on the ellipsoid whose magnetization should be switched. The field is turned off after t = 4:8ns in order to transfer the magnetic charge to the next vertex controlling the propagation. (c)-(e) Schematic illustration of the monopole (dark blue) propagation. (f)-(h) Snapshots of the magnetization states from the output of the conducted micromagnetic simulations, where f) illustrates the initial and g) the final magnetic configurations. The

magnetization evolution during the simulations is depicted at different times (white boxes) in h). Color in f)-h) shows the x-component of the magnetization, as given by the colorbar.

Supplementary Files

This is a list of supplementary files associated with this preprint. Click to download.

- KoraltanSuppMat.pdf
- YPropagationwithfields.gif
- SMMEPs.gif
- StepwiseXpropagation0to115ns.gif